Neurobiology of Aging 84 (2019) 41–49

Contents lists available at ScienceDirect

Neurobiology of Aging

journal homepage: www.elsevier.com/locate/neuaging

Sulcal morphology in Alzheimer's disease: an effective marker of diagnosis and cognition

Maxime Bertoux [a,b,*], Julien Lagarde [b,c,1], Fabian Corlier [d,1], Lorraine Hamelin [b,c], Jean-François Mangin [e], Olivier Colliot [f], Marie Chupin [f], Meredith N. Braskie [d], Paul M. Thompson [d], Michel Bottlaender [c,e], Marie Sarazin [b,c]

[a] Univ Lille, Inserm, CHU Lille, UMR 1171, Degenerative and Vascular Cognitive Disorders, Lille, France
[b] Unit of Neurology of Memory and Language, Université Paris Descartes, Sorbonne Paris Cité, Centre Hospitalier Sainte Anne, Paris, France
[c] UMR 1023 IMIV, Service Hospitalier Frédéric Joliot, CEA, Inserm, Université Paris Sud, CNRS, Université Paris-Saclay, Orsay, France
[d] Imaging Genetics Center, USC Stevens Neuroimaging and Informatics Institute, Keck School of Medicine of USC, University of Southern California, USA
[e] Neurospin, CEA, Gif-sur-Yvette, France
[f] Institut du Cerveau et de la Moelle épinière, ICM, Inserm, Sorbonne Universités, UPMC Univ Paris 06, Paris, France

ARTICLE INFO

Article history:
Received 25 October 2018
Received in revised form 23 July 2019
Accepted 24 July 2019
Available online 29 July 2019

Keywords:
Alzheimer's disease
Sulcal morphology
Cortical thickness
Sulcal width
Data-driven science

ABSTRACT

Measuring the morphology of brain sulci has been recently proposed as a novel imaging approach in Alzheimer's disease (AD). We aimed to investigate the relevance of such an approach in AD, by exploring its (1) clinical relevance in comparison with traditional imaging methods, (2) relationship with amyloid deposition, (3) association with cognitive functions. Here, 51 patients (n = 32 mild cognitive impairment/mild dementia-AD, n = 19 moderate/severe dementia-AD) diagnosed according to clinical-biological criteria (CSF biomarkers and amyloid-PET) and 29 controls (with negative amyloid-PET) underwent neuropsychological and 3T-MRI examinations. Mean sulcal width (SW) and mean cortical thickness around the sulcus (CT-S) were automatically measured. We found higher SW and lower CT-S in patients with AD than in controls. These differences were more pronounced at later stages of the disease and provided the best diagnostic accuracies among the imaging markers. Correlations were not found between CT-S or SW and amyloid deposition but between specific cognitive functions and regional CT-S/SW in key associated regions. Sulcal morphology is a good supporting diagnosis tool that reflects the main cognitive impairments in AD. It could be considered as a good surrogate marker to evaluate the efficacy of new drugs.

1. Introduction

Although positron emission tomography (PET) imaging now enables in vivo detection of amyloid (Klunk et al., 2004) and tau (Villemagne et al., 2015) lesions, these techniques are more invasive and expensive than magnetic resonance imaging (MRI) as well as less widely available. Furthermore, the ATN classification system ("A" [Aβ-amyloid], "T" [tau], and "N" [neuronal injury]) proposed recently by the United States' National Institute on Aging and Alzheimer's Association (NIA-AA) research framework reinforced the role of anatomic MRI as a marker of neurodegeneration (N), in addition to amyloid and tau (A, T) markers (Jack et al., 2018). This stresses the importance to refine the methods used to analyze structural brain MRI because of the supportive role they have in the diagnosis of neurodegenerative diseases such as Alzheimer's disease (AD).

As an example, hippocampal volume measurement has long been considered to be a supportive diagnostic feature of AD (Albert et al., 2011; Dubois et al., 2014). Indeed, hippocampal volume (HV) correlates with memory performance (Sarazin et al., 2010), the density of neurofibrillary tangles at autopsy (Jack et al., 2002), and cerebrospinal fluid (CSF) levels of tau and phosphorylated tau (de Souza et al., 2012), which are all markers of the underlying pathophysiological processes of AD. However, the overlap between healthy controls and AD patients on HV

* Corresponding author at: Univ Lille, Inserm, CHU Lille, UMR 1171, Degenerative and Vascular Cognitive Disorders, F-59000 Lille, France. Tel.: +33(0)320446021; fax: +33(0)320446022.
E-mail address: maxime.bertoux@inserm.fr (M. Bertoux).
[1] These authors contributed equally.

0197-4580/$ – see front matter
https://doi.org/10.1016/j.neurobiolaging.2019.07.015

measures (de Souza et al., 2013; Frisoni et al., 1999), limits its relevance for diagnostic purpose at the individual level (Frisoni et al., 2010). In addition, hippocampal atrophy is also observed in other neurodegenerative conditions such as frontotemporal dementia (de Souza et al., 2013; Hornberger et al., 2012; La Joie et al., 2013), warranting caution for considering this anatomical marker as specific of AD.

Other quantitative MRI techniques, such as voxel-based morphometry (VBM) and cortical thickness (CT) measures are additional potential tools for the diagnosis of AD as they reveal the involvement of neurodegeneration in the neocortex at an early stage of AD (Cuingnet et al., 2011; Hämäläinen et al., 2007; Holland et al., 2009; Karas et al., 2004; Kinkinghéhum et al., 2008; Singh et al., 2006). CT analyses led to the definition of a cortical atrophy signature of AD consisting in 9 regions showing significant cortical thinning from the early stages of the disease (Dickerson et al., 2009). This signature predicted the conversion from mild cognitive impairment (MCI) to AD dementia (Bakkour et al., 2009) and the progression to AD among cognitively healthy older adults (Dickerson et al., 2011). Based on these methods, clinical classifiers have also been obtained by applying machine learning techniques to structural MRI data (Mateos-Pérez et al., 2018).

Beyond these approaches, measuring the morphology of sulcal cortical folds using three-dimensional processing techniques has been recently proposed as a novel approach to investigate the morphology of the cortical surface (Mangin et al., 2004b, Mangin and Jouvent, 2010), including in AD (Cai et al., 2017; Hamelin et al., 2015). In contrast to VBM or CT measurements, this method is not dependent on gray/white contrast, which weakens with age and disease progression, but on the contrast between the gray matter and the CSF, which is far less affected by these parameters. Sulcal morphology measures provide individual models of cortical anatomy rather than relying on a common stereotaxic space, potentially overcoming some biases induced by spatial normalization (Mangin et al., 2004a). Moreover, the sulcal abnormalities integrate not only atrophy of the cortical mantle around the sulcus but also atrophy of the surrounding gyral white matter, which could enhance the sensitivity to detect the earliest stages of AD (Liu et al., 2013a,b). These measures can lead to a high number of variables, by mapping the cortex into circumscribed and numerous regions of interest, which could have a true relevance in data-driven medicine in the era of big-data and precision medicine in addition to providing high spatial resolution.

So far, only few studies have analyzed sulcal morphology in AD. Despite conflicting results, findings suggest that sulcal morphology analysis provides insights into the structural brain changes in AD (Cai et al., 2017; Im et al., 2008; Liu et al., 2012; Reiner et al., 2012). To our knowledge, only one study based the inclusion of patients and controls on biological evidences of AD (Hamelin et al., 2015). In that study, we showed that sulcal width measures improved the diagnosis of early-onset AD. However, whether sulcal morphology measures improve AD diagnosis in comparison to more traditional MRI methods such as HV, regional cortical thickness, or volumes measures remains unclear. Another unsolved question is how sulcal morphology relates to amyloid deposition and cognitive dysfunctions as so far, correlations between these measures and cognitive scores have never been performed.

The present study aimed to investigate sulcal morphology measurements in AD patients defined by clinical-biological criteria to (a) describe the sulcal morphology profile at both the MCI/mild dementia and moderate/severe dementia stages; (b) compare their accuracy to identify AD pathophysiology in comparison with more broadly used imaging methods; (c) explore their relationship with cortical amyloid deposition and; (d) with specific cognitive dysfunctions in AD.

2. Methods

2.1. Participants

Eighty participants were included from the Biomage (NCT01095744) and ImaBio3 studies (NCT01775696) that were approved by the Ethics Committee of the Pitié-Salpêtrière Hospital. All participants provided signed informed consent and were followed up for 24 months to improve the diagnostic accuracy. Exclusion criteria were (a) any clinical or neuroimaging evidence of focal lesions; (b) severe cortical or subcortical vascular lesions (Fazekas score >1, evaluated on FLAIR sequences); (c) severe depression (score at the Montgomery-Åsberg Depression Rating Scale <30); Montgomery et al., (1979).

Fifty-one typical (i.e., amnestic) AD patients were included according to these criteria: (a) memory impairment observed at the Free and Cued Selective Reminding Test (FCSRT), with or without another cognitive impairment (Sarazin et al., 2007); (b) biological evidence of AD-related pathophysiological process as defined by a CSF biomarker profile indicative of AD (Innotest Amyloid Tau Index score <0.8) analyzed in 86% (n = 44/51) of patients (de Souza et al., 2011a) and/or positive amyloid imaging on positron emission tomography using ^{11}C-labeled Pittsburgh Compound B (PiB-PET) defined by a global cortical index (GCI) > 1.4 (100%, n = 51/51). Innotest Amyloid Tau Index score was calculated following this formula: $(A\beta_{1-42}) / (240 + 1.18^{*}Tau)$. Patients were divided in 2 groups: MCI due to AD or mild AD dementia (MCI/mildAD, n = 32, 63%) and moderate to severe dementia patients (DemAD, n = 19, 37%) according to the ability to function independently, following the NIA-AA guidelines (Albert et al., 2011; McKhann et al., 2011), and the MMSE score (≥20 or <20, respectively). Twenty-nine healthy controls were included according to these criteria: (a) normal neuropsychological assessment, (b) no history of psychiatric/neurological conditions, and (c) negative amyloid retention on PiB-PET (GCI < 1.4).

2.2. Neuropsychological measures

All participants underwent a neuropsychological examination that included the MMSE (Folstein et al., 1975) and a standard evaluation of verbal (FCSRT) and visual long-term memory (recall of Rey complex figure), executive functions (Trail Making Task, similarities from WAIS III), working memory (digit spans), language (word naming task), gesture praxis, and visuoconstructive functions (copy of Rey figure).

2.3. Imaging parameters

2.3.1. MRI acquisition

MRI scans were obtained on a 3T Siemens Trio scanner (32 channels with a 12 channel head coil for signal reception) involving a 3D T1-weighted volumetric magnetization-prepared rapid-gradient echo (MP-RAGE) sequence with repetition time = 2300 ms, echo time = 2.98 ms/3.43, inversion time = 900, matrix = 256 × 256, and slice thickness = 1 mm. This sequence provided a high gray/white matter contrast-to-noise ratio and allowed excellent segmentation and coregistration with the PET images.

2.3.2. Sulcal morphometry measures

For each participant, cortical sulci were reconstructed and automatically identified from each individual 3D T1-weighted MRIs. As performed in a previous study (Hamelin et al., 2015), the cortical sulci were extracted from T1-weighted scans via the following steps. First, a brain mask was obtained with the SPM8

skull-cleanup tool, an automated skull stripping procedure. Second, segmentation of the images into gray and white matter as well as CSF was performed using histogram scale-space analysis and mathematical morphology (Mangin et al., 2004a,b). Third, individual sulci were segmented and labeled using Morphologist from BrainVISA (http://brainvisa.info/web/morphologist.html). For segmentation, a kind of crevasse detector was used to reconstruct each fold geometry as the medial surface from the 2 opposing gyral banks that spanned from the most internal point of the fold to the convex hull of the cortex (Mangin et al., 2004a,b). Then, a Bayesian-inspired pattern recognition approach relying on statistical probabilistic anatomy maps and multiscale spatial normalization was used to label the folds for 60 sulci (Perrot et al., 2011; Mangin et al., 2015). The sulcal width (SW) was quantified for each sulcus using the average distance between both banks of the pial surface. This average distance was computed as a ratio between the volume of CSF filling up the sulcus from the brain hull to the fold bottom, and the surface area of the sulcus estimated by half the sum of the areas of the triangles making up a mesh of the corresponding medial surface. A fast-marching algorithm applied to a voxel-based binary representation of the cortex gray matter was used to compute the average thickness of the cortical mantle on both sides of the sulcus (CT-S). Both measures were computed in millimeters for each participant as individual values in each region of interest (ROI) for each hemisphere. Quality checks were performed at each step of the procedure. No manual corrections were needed. Additional details about this procedure and the quality checks performed are provided in the Supplementary material.

We defined 18 ROIs, which were extracted in each brain hemisphere (Fig. 1). In the frontal lobe: the (**1**) anterior lateral sulci (superior, middle, intermediate, and inferior frontal sulci), (**2**) median frontal sulci (medial portions of the inferior-frontal sulcus, inferior-rostral-frontal sulcus, and anterior callosomarginalis fissure), (**3**) orbital sulci (polar-frontal, orbital, and olfactory sulci), (**4**) internal frontal sulcus, (**5**) subcallosal sulcus (or corpus callosum sulcus, including its nonfrontal parts), (**6**) precentral sulci (lateral portions of the superior, middle, and inferior frontal sulci), and (**7**) central sulcus. Within the temporal lobe: the (**8**) temporo-polar, (**9**) superior temporal, (**10**) inferior temporal, (**11**) rhinal, (**12**) collateral, and (**13**) temporo-occipital sulci, grouped with their branches. In the parietal lobe: the (**14**) lateral parietal sulci (intraparietal sulcus, superior and inferior postcentral sulci, superior parietal sulcus, and their intermediate branches), (**15**) precuneus and retrosplenial sulci (including the internal parietal and medial inferior parietal sulci), (**16**) posterior cingulate sulci (including the posterior callosomarginalis and paracentral sulci), and (**17**) parieto-occipital sulcus. In the occipital lobe, we grouped all sulci into a unique ROI defined as (**18**) occipital sulci.

2.3.3. Regional cortical volumes (rVOIs)

Gray matter automated segmentation was performed from each individual 3D-T1-weighted MRI scan using the VBM8 package of SPM8 (Institute of Neurology, London, UK; http://www.fil.ion.ucl.ac.uk/spm/). The automated anatomical labeling atlas was deformed to each individual MRI (deformation field extracted from VBM8) and intersected with the T1-MRI gray matter. We pooled the AAL VOIs into greater volumes of interest, that is (1) frontal; (2) anterior cingulate; (3) middle cingulate; (4) posterior cingulate; (5) precuneus and retrosplenial; (6) parietal; (7) temporal; (8) hippocampus; (9) and occipital VOIs. VOIs were computed for each hemisphere, resulting in 18 rVOIs. Additional details about rVOIs are provided in the Supplementary material.

2.3.4. FreeSurfer cortical thickness (FCT)

A surface-based cortical thickness estimation using the FreeSurfer analysis toolbox (version 5.3; http://surfer.nmr.mgh.harvard.edu/) was performed. A surface-based approach provides better reliability on 2 different same-day scans than voxel-based approaches, and morphometric procedures have been demonstrated to show good test-retest reliability (Clarkson et al., 2011; Han et al., 2006; Reuter et al., 2012). Detailed documentation is available on the FreeSurfer web page. These extracted values were considered for intergroup statistical comparisons. We visually inspected the FreeSurfer parcellation results to identify global segmentation abnormalities including non–cortical tissue labeling, missing structures, and movement artifacts.

Mean cortical thickness indices for 68 ROIs were obtained. We performed quality control review of all cortical regions to ensure accurate labeling of grey-white matter boundaries. Please see the Supplementary material for additional detail about FreeSurfer segmentation and parcellation procedures, the ROIs considered and the full description of the quality check procedure regarding the ROIs approach. One-tailed student tests (controlled for age) were performed for each of the 68 ROIs testing the hypothesis that the average thickness in a given ROI is smaller in AD participants. We controlled for multiple comparisons by controlling the false discovery rate at 5%, using the Benjamini and Yekutieli procedure under the assumption of positive dependency between variables, to determine in which ROIs the differences between groups were significant (Benjamini et al., 2001).

In parallel to the ROI approach, we used FreeSurfer's built-in statistical tools for vertexwise generalized linear models on the individual surfaces previously resampled into the common anatomic space and smoothed using a Gaussian smoothing kernel of 10 mm. The group comparison (controlled for age) consisted of AD participants versus controls. The statistical significance of between-group cortical thickness differences was evaluated using a clusterwise correction for multiple comparisons (Hagler et al.,

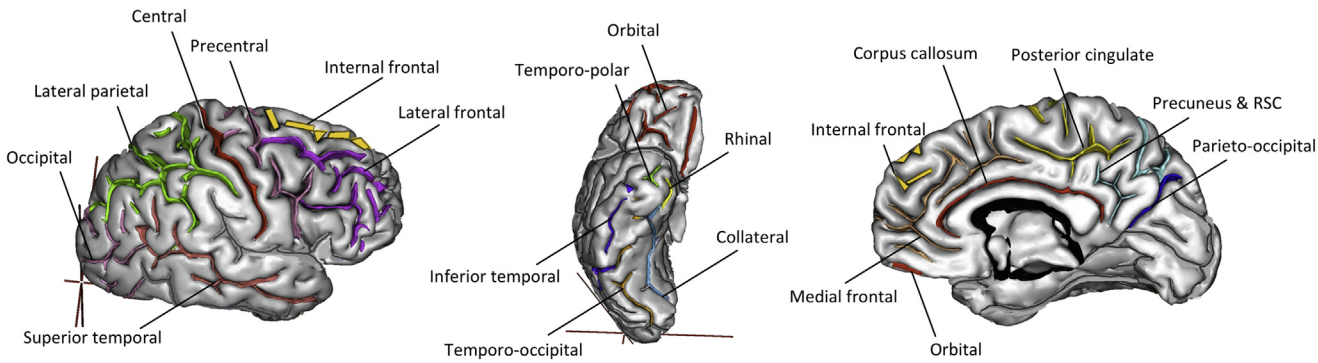

Fig. 1. Representation of the main sulci analyzed, pooled into the 18 regions of interest defined (lateral, medial, and inferior views of the right hemisphere).

2006). Initial clusters of significant contiguous groups of vertices were obtained using a vertexwise p-value threshold of $p < 0.01$ (one-tailed) and were only reported if they met a clusterwise forming threshold (Cluster Simulation Data probability) of $p < 0.05$ (one-tailed), accounting for the probability of finding a given cluster by chance, given its surface area and the amount of smoothing applied to surface maps. Individual thickness averages were then obtained within each significant cluster and subsequently normalized by their surface area and averaged to arrive at an individual thickness index for each participant.

2.3.5. Hippocampal volume

Hippocampal segmentation was performed bilaterally for each participant using the validated software SACHA (Segmentation Automatisée Compétitive de l'Hippocampe et de l'Amygdale) (Chupin et al., 2009; de Souza et al., 2013). Briefly, this software segments the hippocampus and the amygdala on the basis of competitive region-deformation between these structures, relying on prior knowledge of the relative positions of these structures with respect to 11 sets of anatomical landmarks automatically identified at the border of the deforming objects. A quality check of the segmentation was performed and passed for all participants. Only the hippocampal volume was considered.

2.3.6. Regional amyloid load

[^{11}C]-PIB PET scans were performed on a high-resolution tomograph (CTI/Siemens Molecular Imaging, TN). Quantitative analysis was performed as described previously (de Souza et al., 2011b). Briefly, parametric images representing [^{11}C]-PIB uptake in each voxel was calculated as a region-to-cerebellum ratio of the radioactivity concentration over 40–60 minutes. The AAL VOIs defined previously were applied on the PET parametric images after coregistration with the participant's MRI. The GCI of [^{11}C]-PIB uptake was defined as the participant's mean value in the neocortical regions cited previously; see Section 2.3.3. Additional details are provided on PET imaging and the computation of regional amyloid burden values in the Supplementary material.

2.4. Statistical analyses

Data were analyzed using SPSS20 (SPSS Inc, Chicago, IL, USA).

2.4.1. Between-groups differences

Three-way then two-by-two differences between groups (controls, MCI/mildAD, demAD) were explored using a multivariate analysis of variance, with age set as a nuisance covariate. All imaging parameters (CT-S, SW, rVOIs, and HV) were adjusted for each participant's intracranial volume derived from SPM8 segmentations preliminary to these analyses, except FCT, which is not affected by intracranial volume (Barnes et al., 2010). Differences were sought for clinical, neuropsychological, demographical, and the imaging measures. False discovery rate (FDR) corrections were applied to account for multiple comparisons.

2.4.2. Prediction of AD diagnosis

A data-driven method was applied to identify the set of ROIs that was the best predictor (in %) of the presence/absence of AD (controls vs. patients) diagnosis among the imaging measures that involved multiple regions (CT-S/SW/rVOIs/FCT). The same analysis was applied for HV measure. This automated procedure relied on a binary logistic regression where variables provided by each method were included in the analysis then removed stepwise from the model according to a probability of Wald statistic unless they yielded a significant contribution to the model ($p < 0.001$). Bootstrap procedures were conducted (with a total of 1000 resamplings with a 95% confidence interval) to ensure the stability of each classification performed. This approach was complemented by the computation of sensitivity, specificity, and (95%) confidence intervals, all calculated based on the number of true/false positive and true/false negative obtained with the logistic regression output. The application of Akaike's information criterion (AIC) allowed us to compare the accuracy of each imaging methods' prediction power, independently of the number of predictors.

2.4.3. Correlations with amyloid load and cognitive performance

Principal component analyses (PCA) were run in AD patients (all) with CT-S and SW values as well as with neuropsychological scores, after a z-score transformation to reduce the data sets. Correlations between sulcal (CT-S or SW) components and amyloid deposition or neuropsychological components were sought with age as a nuisance covariate. Automated linear modeling was also performed to quantify the percentage of variance of the different neuropsychological components explained by the variation of the different sulcal components.

3. Results

3.1. Demographics, clinical, biological

Age, education, and gender did not differ across the 3 groups (all $p > 0.10$). No differences were observed between MCI/mildAD and DemAD on CSF levels of phospho-tau, total-tau, and beta-amyloid, or amyloid load GCI measured by PET. For the last analysis, the delay between the lumbar puncture and the PET was set as a covariate (Table 1).

3.2. Neuropsychological comparisons

As expected, ANOVA showed significant differences between the 3 groups on the MMSE and all neuropsychological scores, following the expected pattern controls>MCI/mildAD>demAD. (Supplementary Table 2)

3.3. Intergroup comparisons on imaging measures

All the analyses were conducted with age as a nuisance covariate and were FDR corrected.

For ***CT-Ss***, the comparisons between MCI/mildAD or DemAD and controls are shown in Supplementary Table 3 and Fig. 2. When contrasting AD subgroups, no significant results survived after FDR

Table 1
Demographics, clinical and diagnostic biomarker measures for controls, MCI or mild AD (MCI/mildAD) and moderate/severe (demAD) patients

	Controls	MCI/mildAD	DemAD
N (M/F)	29 (15/14)	32 (13/19)	19 (8/11)
Age	65.82 (7.59)	66.59 (10.03)	68.10 (11.60)
Education	12.70 (3.05)	13.47 (3.59)	11.59 (4.00)
CDR	0	0.5	1 (n = 17), 2 (n = 2)
MMSE	29.22 (0.93)	23.59 (2.9)[a,b]	15.84 (4.19)[a,b]
Biomarkers			
CSF Ab42	N.A.	334.52 (95.46)	262.81 (106.82)
CSF Tau	N.A.	657.48 (208.18)	618.73 (319.41)
CSF pTau	N.A.	94.70 (23.37)	91.23 (42.82)
Amyloid PET (GCI)	1.22 (0.07)	2.64 (0.42)[a]	2.57 (0.51)[a]

Key: MCI, mild cognitive impairment; CSF, cerebrospinal fluid; CDR, Clinical Dementia Rating; GCI, global cortical index.
[a] Significant difference in comparison with controls.
[b] Significant difference between AD groups.

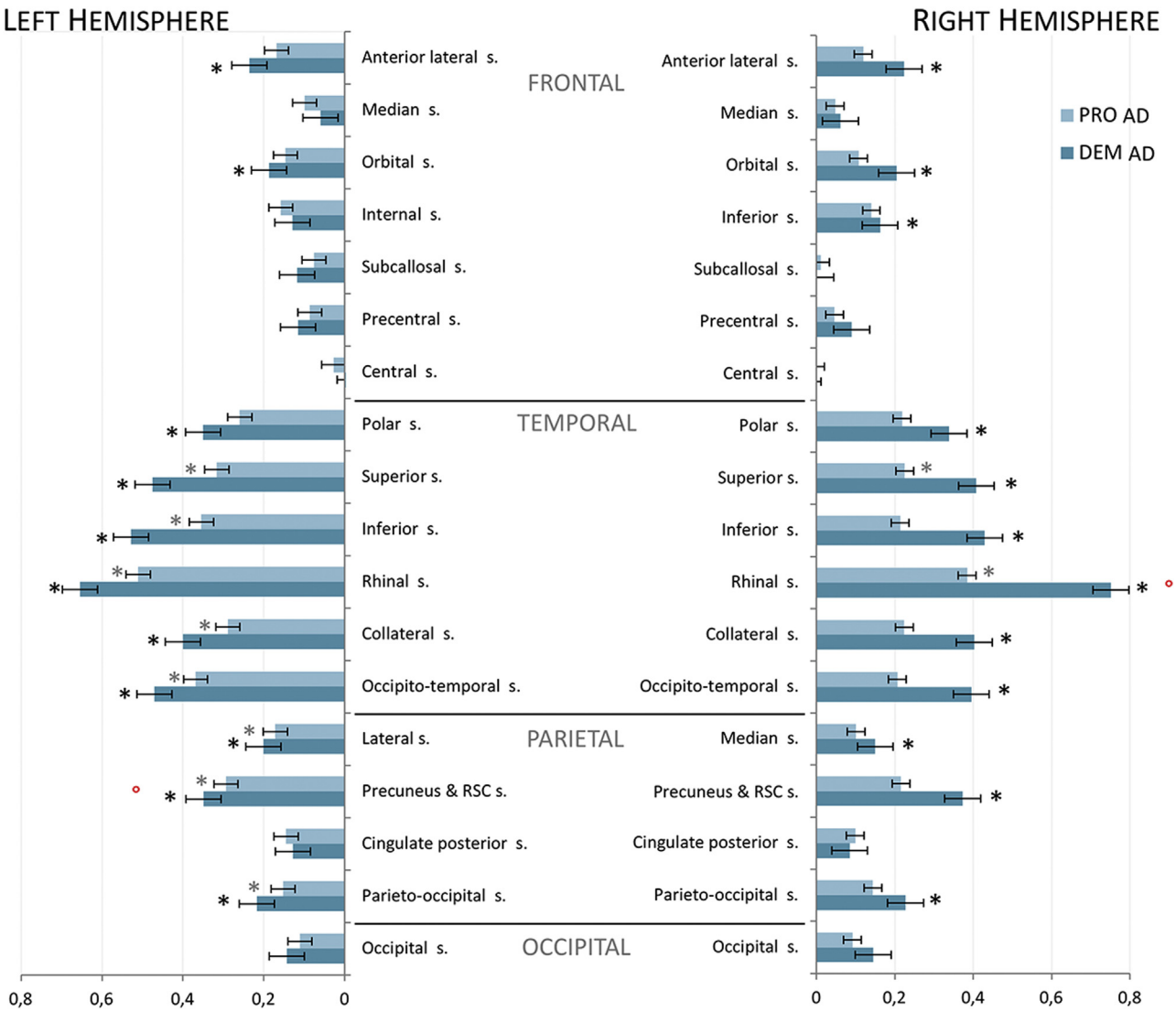

Fig. 2. CT-S reduction (in mm) in MCI/mildAD and DemAD patients compared with controls in each of the 18 ROIs of each hemisphere. Gray stars above MCI/mildAD bars represent significant differences ($p < 0.05$ FDR corrected) between MCI/mildAD patients and controls, black stars above DemAD bars represent significant differences ($p < 0.05$ FDR corrected) between DemAD patients and controls, and red circles represent significant but uncorrected differences ($p < 0.05$) between MCI/mildAD and DemAD patients. Abbreviations: AD, Alzheimer's disease; MCI, mild cognitive impairment; FDR, false discovery rate. (For interpretation of the references to color in this figure legend, the reader is referred to the Web version of this article.)

correction but uncorrected decreases were observed in the left precuneus and right rhinal sulcus (all p's < 0.01) in DemAD.

For ***SW***, the comparisons between MCI/mildAD or DemAD and controls are shown in Supplementary Table 3 and Fig. 3. When contrasting AD subgroups, no significant results survived after FDR correction but SW was higher in the left precuneus, collateral fissure, right occipitotemporal, central sulci, and anterior lateral fissure in DemAD (all p's < 0.05).

For **rVOIs** (Supplementary Table 4), MCI/mildAD showed lower cortical volume in the bilateral frontal, bilateral hippocampus, right precuneus, right parietal, and right temporal regions ($p < 0.05$) in comparison with controls. DemAD showed lower cortical volume in the bilateral parietal ($p < 0.0005$), left middle cingulate, right anterior cingulate, right precuneus, right temporal, and right occipital regions ($p < 0.05$) compared with controls. Results of the contrast between the AD groups are presented on Supplementary Table 5.

For **FCT**, the comparisons between MCI/mildAD or DemAD and controls are shown in Supplementary Table 6. Between the AD groups (Supplementary Table 7), DemAD showed lower FCT than MCI-AD in the following ROIs: bilateral superior, inferior (including supramarginal gyrus) and medial (precuneus) parietal, extending to the right isthmus of the cingulate cortex, and the lateral occipital. DemAD also showed lower FCT than MCI/mildAD in lateral (left inferior, bilateral middle, left superior, and right transverse), inferior (right fusiform) and medial (parahippocampal) temporal ROIs. Lower FCT in the left precentral and pars opercularis ROIs was also observed in DemAD.

For ***HV***, MCI/mildAD and DemAD showed smaller left, right, and mean HV (all $p < 0.0001$) compared with controls. No differences were observed between AD subgroups ($p > 0.27$).

3.4. Automated identification of the best imaging predictors

An automated binary logistic regression (stepwise) analysis was used to identify the group of measures that was the best predictor of an AD diagnosis within each set of measures (CT-S, SW, rVOIs,

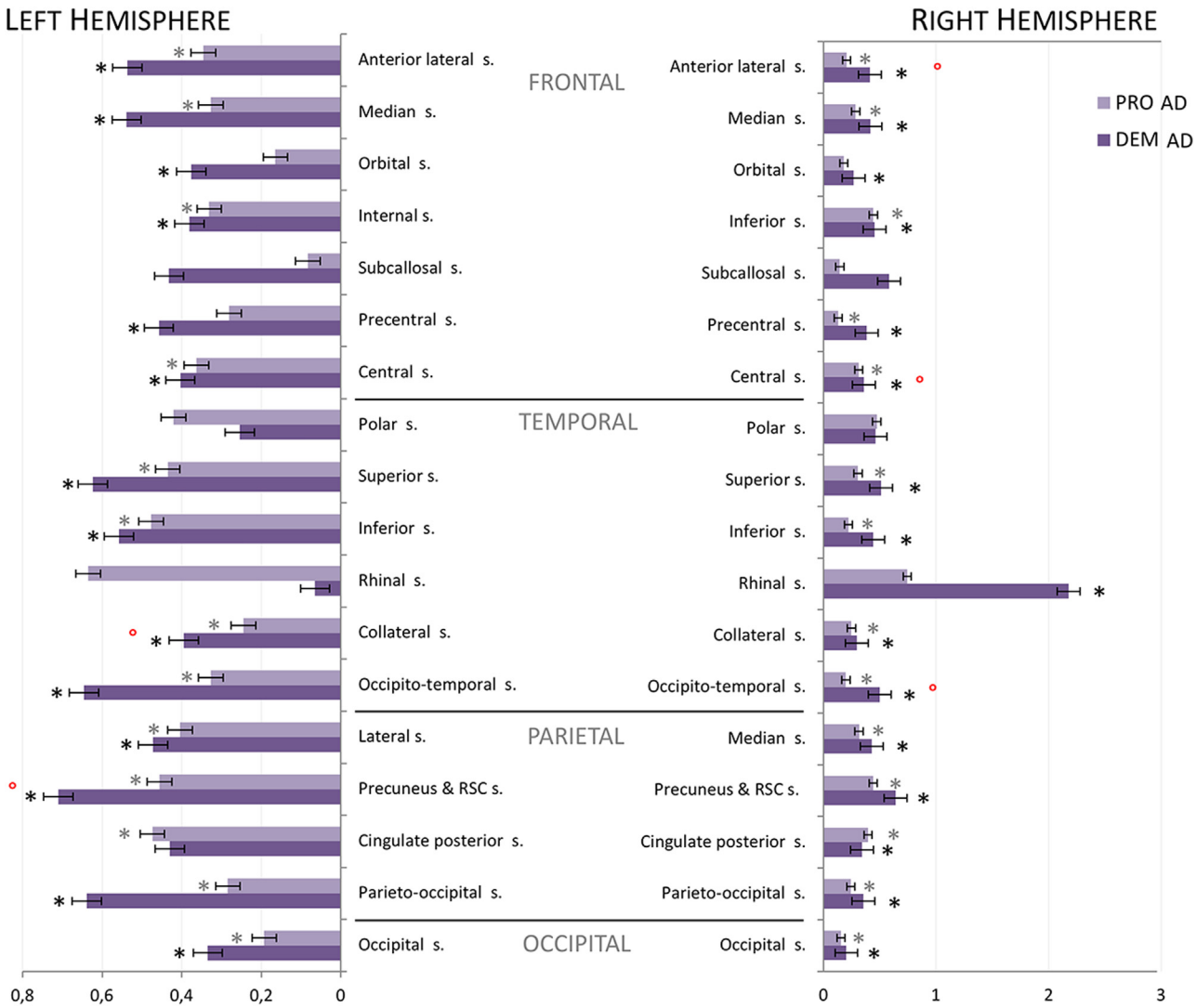

Fig. 3. SW increase (in mm) in MCI/mildAD and DemAD patients compared with controls in each of the 18 ROIs of each hemisphere. Gray stars above MCI/mildAD bars represent significant differences ($p < 0.05$ FDR corrected) between MCI/mildAD patients and controls, black stars above DemAD bars represent significant differences ($p < 0.05$ FDR corrected) between DemAD patients and controls, and red circles represent significant but uncorrected differences ($p < 0.05$) between MCI/mildAD and DemAD patients. Abbreviations: AD, Alzheimer's disease; SW, sulcal width; FDR, false discovery rate; MCI, mild cognitive impairment. (For interpretation of the references to color in this figure legend, the reader is referred to the Web version of this article.)

FCT), independently from the patients' disease stages. This automated and whole-brain approach allowed an analysis independent from any a priori hypothesis (Table 2).

For ***CT-S***, the binary logistic regression identified a set of 7 ROIs that was the best significant predictor of an AD diagnosis (90.8%; −2log-likehood = 26.94; $p < 0.000001$); it included the left inferior temporal, left central, right superior temporal, right polar temporal, right inferior temporal, right rhinal, and right medial frontal sulci. This set of imaging variables provided a sensitivity of 94.2% (CI (95%): 87.7–100.6) and a specificity of 85.2% (CI: 71.8–98.6).

For ***SW***, the set of regions that was the best significant predictor of an AD diagnosis (92.1%; −2log-likehood = 24.89; $p < 0.000001$) was composed from 8 regions including the left inferior temporal, internal frontal, anterior lateral frontal and the right rhinal, polar temporal, internal frontal, collateral, and anterior lateral frontal sulci. This result was associated with a sensitivity of 94.1% (CI: 87.7–100.6) and a specificity of 88.9% (CI: 77.0–100.7). When both (CT-S and SW) types of measures were considered in a single model, the regression overfitted and failed to provide results.

For ***rVOIs***, the identified group (82.1%; −2log-likehood = 49.49 $p < 0.000001$) was composed of the left anterior cingulate and the right frontal, middle, and posterior cingulate gyri, precuneus, parietal, temporal, and posterior rVOIs. This provided a sensitivity of 90.2% (CI: 82.0–98.4) and a specificity of 66.7% (CI: 48.9–84.5).

For ***FCT***, owing to the large number of ROIs considered (n = 68) and the relatively small sample size (n = 80), the regression model

Table 2
Prediction accuracy (in %) with Akaike's information criterion (AIC) value in bracket of the diagnosis of AD for sulcal morphometry (sulcal cortical thickness and width), regional cortical volume, FreeSurfer cortical thickness, and hippocampal volume measures

Imaging measures	Accuracy to predict AD
Sulcal cortical thickness (CT-S)	90.8% (42.94)
Sulcal width (SW)	92.1% (42.89)
Regional cortical volumes (rVOIs)	82.1% (67.49)
FreeSurfer cortical thickness (FCT)	80.8% (75.98)
Hippocampal volume (HV)	78.9% (65.76)

Higher percentages and lower AICs indicate better prediction accuracy.

overfitted and failed to provide any results. A different approach was then used to ensure a comparison with FreeSurfer's data: we considered the regions in which the cortical thickness was decreased in AD (vs. controls) based on the vortexwise comparison made. During this analysis, 6 regions (namely the left inferior temporal, isthmus cingulate, superior frontal, and the right supramarginal, inferior parietal, and precuneus) were identified by FreeSurfer (raw data presented on Supplementary Table 8; results showed on Fig. 2). These regions were then included in the logistic regression model using enter method. This group reached an accuracy of 80.8% (−2log-likehood = 61.98 $p < 0.000001$). This provided a sensitivity of 83.3% (CI: 70.2–91.6) and a specificity of 75.0% (CI: 52.9–89.3).

For ***HV***, the regression reached 78.9% of accuracy (−2log-likehood = 61.764 $p < 0.00005$), with a sensitivity of 86.0% (CI: 73.3–94.2) and a specificity of 65.4% (CI: 44.3–82.8).

To ensure the stability of these classifications analyses, we performed bootstrapping and obtained identical results for all sets of imaging variables considered. As shown in Table 2, despite high accuracy for all methods considered, AIC values indicate that sulcal measures are better predictors of AD.

3.5. Correlations with amyloid load

There was no correlation between regional amyloid load or GCI (PiB binding) and any sulcal measure in both AD subgroups and AD group as a whole.

3.6. Neuropsychological correlates (in patients with AD)

To explore the neuropsychological correlates of sulcal morphology, we ran a PCA on all neuropsychological scores, then on all CT-S or SW measures separately to reduce the dimensions of the data set. Four neuropsychological components were identified with labels deducted from the PCA structure: (1) verbal memory, (2) executive functioning, (3) instrumental, and (4) orientation components (considering the eigenvalue on the scree plot). Reduction of data procedures were also performed for sulcal measures. More specifically, bilateral sulcal data of each lobe for each parameter (CT-S or SW) were considered separately and a PCA was conducted in setting the number of components to extract to 1. Therefore, we obtained frontal, temporal, and parietal components (only a single occipital value was available and thus the PCA was not conducted for this lobe) for each type of parameter. Then, correlations (controlled for age) were sought between the neuropsychological and the CT-S or SW lobar components. These analyses revealed a significant correlation (corrected for multiple comparisons) between (a) the verbal memory and temporal sulcal components ($R = 0.48$; $p < 0.0001$ for CT-S and $R = -0.30$; $p < 0.05$ for SW components), (b) the instrumental and parietal components ($R = 0.39$; $p < 0.005$ for CT-S and $R = -0.51$; $p < 0.00005$ for SW), (c) the executive and both frontal and parietal SW components ($R = -0.50$; $p < 0.0001$; $R = -0.57$; $p < 0.000005$, respectively).

An automated linear model was conducted to investigate the respective contribution of CT-S decrease and SW increase within all ROIs to the neuropsychological component's variance in patients. Results are detailed in Table 3.

4. Discussion

In this study, we investigated sulcal morphology in AD at MCI/mild dementia and moderate/severe dementia stages. We found lower CT-S and higher SW in temporal, parietal, and frontal regions in patients, the differences being more pronounced with the severity of the disease. When we compared the different MRI measures considered in this study, the best diagnostic accuracy to predict AD was obtained with sulcal SW. The more broadly used MRI measures such as HV, regional cortical volumes, or FreeSurfer cortical thickness achieved lower prediction power. In addition, sulcal morphology was not correlated with amyloid load but was associated with specific cognitive deficits. These investigations were conducted in patients/controls with biological confirmation/exclusion of AD diagnosis to confirm/exclude the AD pathophysiological process. In addition, all images were acquired within a standardized protocol on a single MRI machine enabling increased image quality and homogeneity in comparison with multicentre studies (Cuingnet et al., 2011; Plant et al., 2010).

The few studies that have previously analyzed sulcal morphology in AD were based on heterogeneous methods. Some analyzed sulcal changes by averaging all sulcal measures in each lobar region, whereas others chose to consider only a limited number of sulci, selecting the largest ones from different lobes to increase their identification while reducing the interindividual variability. These different studies brought significant evidence for the potential that sulcal measures have for improving the diagnosis of AD. By averaging the bilateral sulcal measures in 18 ROIs and centering our investigation on SW in early- and late-onset AD, we previously observed that SW increase in temporoparietal regions characterized early-onset AD and was a better diagnostic maker than HV in this population (Hamelin et al., 2015).

In the present study, we chose to increase the spatial resolution by defining 18 ROIs in each brain hemisphere and to investigate both CT-S and SW in mild and moderate/severe AD patients. The benefit of such higher spatial resolution approach was counterbalanced by the number of variables to consider statistically. Given the high number of measures that were included in the analyses, we chose to present some neuropsychological correlation results that were not corrected for multiple comparisons. Those were only presented as exploratory results and should be confirmed in an independent sample. In parallel, data reduction strategies such as PCA were adopted to decrease the number of variables (Ming et al., 2015).

Our results confirm that sulcal modifications appear at an early stage during the course of AD and are not circumscribed to limbic structures despite the absence of language, visuospatial or praxis impairment, as if sulcal changes in some regions precede cognitive

Table 3
Respective correlation between CT-S decrease and SW increase within all sulcal ROIs with the neuropsychological components' variance in AD

Neuropsychological component	Regions of CT-S decrease	Regions of SW increase	% Of variance explained
Episodic memory	Left superior temporal, right occipito-temporal, left central sulci and bilateral rhinal sulci	Bilateral internal frontal, left superior temporal, right polar temporal and parieto-occipital sulci	64.4% (all sulcal predictors $p < 0.01$)
Executive functions	Left lateral parietal, left frontal subcallosal, left precentral and central, right rhinal and right orbitofrontal sulci	Left superior temporal and right orbitofrontal sulci	70.0% (all sulcal predictors $p < 0.01$)
Instrumental functions	Right precentral, left central and left lateral parietal sulci	Superior temporal and polar temporal sulci	67.0% (all sulcal predictors $p < 0.01$)

Key: AD, Alzheimer's disease; SW, sulcal width; ROI, region of interest; CT-S, cortical thickness around the sulcus.

deficits, and then increase as the disease progresses. In this framework, the precuneus and retrosplenial cortex, in which we found a significant difference between mild and more severe patients for both SW and CT-S measures, could play a critical role as a marker of disease severity, in accordance with previous work showing that the atrophy of the precuneus was associated with a faster clinical progression of AD (Kinkinghéhum et al., 2008).

To determine the group of sulcal ROIs that could predict the more accurate classification of participants into the AD or control groups, thus reflecting the diagnosis accuracy, we used classification algorithms that led to the automatic identification of a specific set of frontal and temporal regions for CT-S and SW measures, independently from any a priori hypothesis. With the aim of determining which imaging method provided the best accuracy to predict AD, we compared the accuracy attained with sulcal measurements with the one attainted with more broadly used approaches such as regional cortical volumes, FreeSurfer cortical thickness and HV. As we were not able to rule out some relative collinearity among our variables during these regression procedures, we completed these analyses by the computation of sensitivity and specificity rates. CT-S and SW provided the best accuracy to identify AD patients as compared with classical methods. The cortical thickness measures provided by FreeSurfer remained less powerful to identify AD, although we had to use an alternative method to provide results with this particular data set as the model overfitted due to the large number of values considered. Although a similar approach was adopted in past studies to identify AD-signature cortical thickness (e.g., Dickerson et al., 2009), therefore providing an interesting trans-methodological comparison, this specific analysis cannot be considered as purely data-driven and the superiority of sulcal morphological parameters over FreeSurfer cortical thickness should be confirmed in larger populations in a full data-driven study.

We hypothesized that our investigations could have been limited by a possible direct effect of amyloid deposits in the sulci, leading to artificially increased CT-S or decreased SW because of increased amyloid load. This hypothesis would have implied a positive correlation between CT-S and amyloid deposition and a negative correlation between SW and amyloid deposition. However, no significant correlation was found between sulcal measures and total or regional cortical PiB binding, suggesting that amyloid plaques density does not exert a mechanical effect on sulcal morphology.

Finally, the correlations between sulcal morphology and specific cognitive domains were explored. Given the large number of cognitive and sulcal variables, these analyses involved a data reduction through PCA. Results showed significant correlations between verbal memory and temporal sulcal components (with both CT-S and SW), instrumental (denomination and gestural praxis) and parietal (CT-S and SW) components and executive and both parietal and frontal SW components. These analyses were confirmed by automated linear models showing that different sulcal modifications significantly predicted the variance of neuropsychological components. In sum, specific cognitive impairments were associated with regional CT-S decrease and SW increase in key regions involved in memory (temporal cortex), instrumental (parietal cortex), and executive (frontoparietal cortex) processing. These exploratory analyses, relying sometimes on uncorrected results that could limit their generalizability, highlight the clinical interest of sulcal measures. Although these results would need further confirmation through studies that should be specifically designed to assess these relationships with cognitive performance (and thus would require more participants), this is the first time that sulcal morphology modifications are related to cognitive decline. This is of particular importance as markers of neuronal injury have the potential to provide pathologic staging information. In the context of the ATN classification system proposed by the NIA-AA research framework, sulcal morphology measures could provide relevant prediction of future cognitive decline when considered with amyloid and tau biomarkers (Jack et al., 2018). In this perspective, future studies should also assess the ability of sulcal morphology measures to discriminate Aβ+ from Aβ− patients.

Taken together, these results highlight the usefulness of sulcal morphology analyses in AD. They show that sulcal morphology is an efficient imaging marker of AD diagnosis, and related to its cognitive deficits. In addition, the comparisons with controls revealing that sulcal morphology modifications being more severe and more broadly distributed in the brain in later stages of AD suggest that sulcal measures could be sensitive to the severity of the disease. Sulcal morphology could provide a new surrogate marker to evaluate the efficacy of future disease-modifying strategies. As comprehensive and almost fully automatically extracted data set of an individual's brain anatomy, sulcal measures also have relevance for precision medicine and should be considered as new data to be implemented in the clinical projects of big-scale initiative such as Human Brain Project or BRAIN Initiative.

Acknowledgements

The authors are greatly indebted to the chemical/radiopharmaceutical and nursing staff of Service Hospitalier Frédéric Joliot for the synthesis of the ^{11}C-PIB and patient management, and to the CENIR (Centre de Neuroimagerie de Recherche) for patients' management during MRI acquisition. They acknowledge the CATI (Centre de d'Acquisition et de Traitement automatisé de l'Image) for its technical support.

MBe, JL, LH, JFM, OC, MC, FC, and MBo report no conflict of interest. During the two last years, MS has collaborated with Allianz and with the pharmaceutical company Novartis (lecture/speaking).

The study was founded by French Agence Nationale de la Recherche (ANR-07-LVIE-002-01), French Fondation Nationale de Gérontologie and MEDIPAR; French Health Ministry (PHRC-0053-N 2010), Institut Roche de Recherche et Médecine Translationnelle and Fondation pour la Recherche Médicale (to LH).

Authors' contributions: MB, LH, OC, and MS contributed to design of the study. MB, LH, FC, and MC contributed to acquisition of experimental data. JL, LH, MB, and MS contributed to acquisition of clinical data. MB and FC contributed to statistical analysis. MB, JL, MB, OC, and MS contributed to interpretation of results. MB, JL, and MS contributed to manuscript writing. All the authors edited the manuscript.

Appendix A. Supplementary data

Supplementary data to this article can be found online at https://doi.org/10.1016/j.neurobiolaging.2019.07.015.

References

Albert, M.S., DeKosky, S.T., Dickson, D., Dubois, B., Feldman, H.H., Fox, N.C., Gamst, A., Holtzman, D.M., Jagust, W.J., Petersen, R.C., Snyder, P.J., Carrillo, M.C., Thies, B., Phelps, C.H., 2011. The diagnosis of mild cognitive impairment due to Alzheimer's disease: recommendations from the National Institute on Aging-Alzheimer's Association workgroups on diagnostic guidelines for Alzheimer's disease. Alzheimers Dement. 7, 270–279.

Bakkour, A., Morris, J.C., Dickerson, B.C., 2009. The cortical signature of prodromal AD: regional thinning predicts mild AD dementia. Neurology 72, 1048–1055.

Barnes, J., Ridgway, G.R., Bartlett, J., Henley, S.M., Lehmann, M., Hobbs, N., Clarkson, M.J., MacManus, D.G., Ourselin, S., Fox, N.C., 2010. Head size, age and gender adjustment in MRI studies: a necessary nuisance? Neuroimage 53, 1244–1255.

Benjamini, Y., Yekutiely, D., 2001. The control of the false discovery rate in multiple testing under dependency. Ann. Statist. 29, 1165–1188.

Cai, K., Xu, H., Guan, H., Zhu, W., Jiang, J., Cui, Y., Zhang, J., Liu, T., Wen, W., 2017. Identification of early-stage Alzheimer's disease using sulcal morphology and other common neuroimaging indices. PLoS One 12, e0170875.
Chupin, M., Hammers, A., Liu, R.S.N., Liu, R.S., Colliot, O., Burdett, J., Bardinet, E., Duncan, J.S., Garnero, L., Lemieux, L., 2009. Automatic segmentation of the hippocampus and the amygdala driven by hybrid constraints: method and validation. Neuroimage 46, 749–761.
Clarkson, M.J., Cardoso, M.J., Ridgway, G.R., Modat, M., Leung, K.K., Rohrer, J.D., Fox, N.C., Ourselin, S., 2011. A comparison of voxel and surface based cortical thickness estimation methods. Neuroimage 57, 856–865.
Cuingnet, R., Gerardin, E., Tessieras, J., Auzias, G., Lehéricy, S., Habert, M.O., Chupin, M., Benali, H., Colliot, O., Alzheimer's Disease Neuroimaging Initiative, 2011. Automatic classification of patients with Alzheimer's disease from structural MRI: a comparison of ten methods using the ADNI database. Neuroimage 56, 766–781.
de Souza, L.C., Lamari, F., Belliard, S., Jardel, C., Houillier, C., De Paz, R., Dubois, B., Sarazin, M., 2011a. Cerebrospinal fluid biomarkers in the differential diagnosis of Alzheimer's disease from other cortical dementias. J. Neurol. Neurosurg. Psychiatry 82, 240–246.
de Souza, L.C., Corlier, F., Habert, M.O., Uspenskaya, O., Maroy, R., Lamari, F., Chupin, M., Lehéricy, S., Colliot, O., Hahn-Barma, V., Samri, D., Dubois, B., Bottlaender, M., Sarazin, M., 2011b. Similar amyloid-β burden in posterior cortical atrophy and Alzheimer's disease. Brain 134, 2036–2043.
de Souza, L.C., Chupin, M., Lamari, F., Jardel, C., Leclercq, D., Colliot, O., Lehéricy, S., Dubois, B., Sarazin, M., 2012. CSF tau markers are correlated with hippocampal volume in Alzheimer's disease. Neurobiol. Aging 33, 1253–1257.
de Souza, L.C., Chupin, M., Bertoux, M., Lehéricy, S., Dubois, B., Lamari, F., Le Ber, I., Bottlaender, M., Colliot, O., Sarazin, M., 2013. Is hippocampal volume a good marker to differentiate Alzheimer's disease from frontotemporal dementia? J. Alzheimers Dis. 36, 57–66.
Dickerson, B.C., Bakkour, A., Salat, D.H., Feczko, E., Pacheco, J., Greve, D.N., Grodstein, F., Wright, C.I., Blacker, D., Rosas, H.D., Sperling, R.A., Atri, A., Growdon, J.H., Hyman, B.T., Morris, J.C., Fischl, B., Buckner, R.L., 2009. The cortical signature of Alzheimer's disease: regionally specific cortical thinning relates to symptom severity in very mild to mild AD dementia and is detectable in asymptomatic amyloid-positive individuals. Cereb. Cortex 19, 497–510.
Dickerson, B.C., Stoub, T.R., Shah, R.C., Sperling, R.A., Killiany, R.J., Albert, M.S., Hyman, B.T., Blacker, D., Detoledo-Morrell, L., 2011. Alzheimer-signature MRI biomarker predicts AD dementia in cognitively normal adults. Neurology 76, 1395–1402.
Dubois, B., Feldman, H.H., Jacova, C., Hampel, H., Molinuevo, J.L., Blennow, K., DeKosky, S.T., Gauthier, S., Selkoe, D., Bateman, R., Cappa, S., Crutch, S., Engelborghs, S., Frisoni, G.B., Fox, N.C., Galasko, D., Habert, M.O., Jicha, G.A., Nordberg, A., Pasquier, F., Rabinovici, G., Robert, P., Rowe, C., Salloway, S., Sarazin, M., Epelbaum, S., de Souza, L.C., Vellas, B., Visser, P.J., Schneider, L., Stern, Y., Scheltens, P., Cummings, J.L., 2014. Advancing research diagnostic criteria for Alzheimer's disease: the IWG-2 criteria. Lancet Neurol. 13, 614–629.
Folstein, S.E., 1975. "Mini-mental state". A practical method for grading the cognitive state of patients for the clinician. J. Psychiatr. Res. 12, 189–198.
Frisoni, G.B., Laakso, M.P., Beltramello, A., Geroldi, C., Bianchetti, A., Soininen, H., Trabucchi, M., 1999. Hippocampal and entorhinal cortex atrophy in frontotemporal dementia and Alzheimer's disease. Neurology 52, 91–100.
Frisoni, G.B., Fox, N.C., Jack Jr., C.R., Scheltens, P., Thompson, P.M., 2010. The clinical use of structural MRI in Alzheimer disease. Nat. Rev. Neurol. 6, 67–77.
Hagler Jr., D.J., Saygin, A.P., Sereno, M.I., 2006. Smoothing and cluster thresholding for cortical surface-based group analysis of fMRI data. Neuroimage 33, 1093–1103.
Hämäläinen, A., Tervo, S., Grau-Olivares, M., Niskanen, E., Pennanen, C., Huuskonen, J., Kivipelto, M., Hänninen, T., Tapiola, M., Vanhanen, M., Hallikainen, M., Helkala, E.L., Nissinen, A., Vanninen, R., Soininen, H., 2007. Voxel-based morphometry to detect brain atrophy in progressive mild cognitive impairment. Neuroimage 37, 1122–1131.
Hamelin, L., Bertoux, M., Bottlaender, M., Corne, H., Lagarde, J., Hahn, V., Mangin, J.F., Dubois, B., Chupin, M., de Souza, L.C., Colliot, O., Sarazin, M., 2015. Sulcal morphology as a new imaging marker for the diagnosis of early onset Alzheimer's disease. Neurobiol. Aging 36, 2932–2939.
Han, X., Jovicich, J., Salat, D., van der Kouwe, A., Quinn, B., Czanner, S., Busa, E., Pacheco, J., Albert, M., Killiany, R., Maguire, P., Rosas, D., Makris, N., Dale, A., Dickerson, B., Fischl, B., 2006. Reliability of MRI-derived measurements of human cerebral cortical thickness: the effects of field strength, scanner upgrade and manufacturer. Neuroimage 32, 180–194.
Holland, D., Brewer, J.B., Hagler, D.J., Fennema-Notestine, C., Dale, A.M., 2009. Alzheimer's Disease Neuroimaging Initiative. Subregional neuroanatomical change as a biomarker for Alzheimer's disease. Proc. Natl. Acad. Sci. U. S. A. 106, 20954–20959.
Hornberger, M., Wong, S., Tan, R., Irish, M., Piguet, O., Kril, J., Hodges, J.R., Halliday, G., 2012. In vivo and post-mortem memory circuit integrity in frontotemporal dementia and Alzheimer's disease. Brain 135, 3015–3025.
Im, K., Lee, J.M., Seo, S.W., Hyung Kim, S., Kim, S.I., Na, D.L., 2008. Sulcal morphology changes and their relationship with cortical thickness and gyral white matter volume in mild cognitive impairment and Alzheimer's disease. Neuroimage 43, 103–113.
Jack, C.R., Dickson, D.W., Parisi, J.E., Xu, Y.C., Cha, R.H., O'Brien, P.C., Edland, S.D., Smith, G.E., Boeve, B.F., Tangalos, E.G., Kokmen, E., Petersen, R.C., 2002. Antemortem MRI findings correlate with hippocampal neuropathology in typical aging and dementia. Neurology 58, 750–757.
Jack, C.R., Bennett, D.A., Blennow, K., Carrillo, M.C., Dunn, B., Haeberlein, S.B., Holtzman, D.M., Jagust, W., Jessen, F., Karlawish, J., Liu, E., Molinuevo, J.L., Montine, T., Phelps, C., Rankin, K.P., Rowe, C.C., Scheltens, P., Siemers, E., Snyder, H.M., Sperling, R., 2018. NIA-AA research framework: toward a biological definition of Alzheimer's disease. Alzheimers Dement. 14, 535–562.
Karas, G.B., Scheltens, P., Rombouts, S.A., Visser, P.J., van Schijndel, R.A., Fox, N.C., Barkhof, F., 2004. Global and local gray matter loss in mild cognitive impairment and Alzheimer's disease. Neuroimage 23, 708–716.
Kinkingnéhun, S., Lehéricy, S., Guichart-Gomez, E., Hergueta, T., Dubois, B., 2008. VBM anticipates the rate of progression of Alzheimer disease: a 3-year longitudinal study. Neurology 70, 2201–2211.
Klunk, W.E., Engler, H., Nordberg, A., Wang, Y., Blomqvist, G., Holt, D.P., Bergström, M., Savitcheva, I., Huang, G.F., Estrada, S., Ausén, B., Debnath, M.L., Barletta, J., Price, J.C., Sandell, J., Lopresti, B.J., Wall, A., Koivisto, P., Antoni, G., Mathis, C.A., Långström, B., 2004. Imaging brain amyloid in Alzheimer's disease with Pittsburgh Compound-B. Ann. Neurol. 55, 306–319.
La Joie, R., Perrotin, A., de La Sayette, V., Egret, S., Doeuvre, L., Belliard, S., Eustache, F., Desgranges, B., Chételat, G., 2013. Hippocampal subfield volumetry in mild cognitive impairment, Alzheimer's disease and semantic dementia. Neuroimage Clin. 3, 155–162.
Liu, T., Lipnicki, D.M., Zhu, W., Tao, D., Zhang, C., Cui, Y., Jin, J.S., Sachdev, P.S., Wen, W., 2012. Cortical gyrification and sulcal spans in early stage Alzheimer's disease. PLoS One 7, e31083.
Liu, T., Sachdev, P.S., Lipnicki, D.M., Jiang, J., Geng, G., Zhu, W., Reppermund, S., Tao, D., Trollor, J.N., Brodaty, H., Wen, W., 2013a. Limited relationships between two-year changes in sulcal morphology and other common neuroimaging indices in the elderly. Neuroimage 83, 12–17.
Liu, T., Sachdev, P.S., Lipnicki, D.M., Jiang, J., Cui, Y., Kochan, N.A., Reppermund, S., Trollor, J.N., Brodaty, H., Wen, W., 2013b. Longitudinal changes in sulcal morphology associated with late-life aging and MCI. Neuroimage 74, 337–342.
McKhann, G.M., Knopman, D.S., Chertkow, H., Hyman, B.T., Jack Jr., C.R., Kawas, C.H., Klunk, W.E., Koroshetz, W.J., Manly, J.J., Mayeux, R., Mohs, R.C., Morris, J.C., Rossor, M.N., Scheltens, P., Carrillo, M.C., Thies, B., Weintraub, S., Phelps, C.H., 2011. The diagnosis of dementia due to Alzheimer's disease: recommendations from the National Institute on Aging-Alzheimer's Association workgroups on diagnostic guidelines for Alzheimer'sdisease. Alzheimers Dement. 7, 263–269.
Mangin, J.-F., Perrot, M., Operto, G., Cachia, A., Fischer, C., Lefèvre, J., Rivière, R., CEA Neurospin, 2015. Sulcus identification and labelling. Brain Mapp. 1, 365–371.
Mangin, J.-F., Poupon, F., Duchesnay, E., Rivière, D., Cachia, A., Collins, D.L., Evans, A.C., Régis, J., 2004a. Brain morphometry using 3D moment invariants. Med. Image Anal. 8, 187–196.
Mangin, J.-F., Rivière, D., Cachia, A., Duchesnay, E., Cointepas, Y., Papadopoulos-Orfanos, D., Scifo, P., Ochiai, T., Brunelle, F., Régis, J., 2004b. A framework to study the cortical folding patterns. Neuroimage 23 (Suppl.1), S129–S138.
Mangin, J.-F., Jouvent, E., 2010. Cachia A In-vivo measurement of cortical morphology: means and meanings. Curr. Opin. Neurol. 23, 359–367.
Mateos-Pérez, J.M., Dadar, M., Lacalle-Aurioles, M., Iturria-Medina, Y., Zeighami, Y., Evans, A.C., 2018. Structural neuroimaging as clinical predictor: a review of machine learning applications. Neuroimage Clin. 20, 506–522.
Ming, J., Harms, M.P., Morris, J.C., Beg, M.F., Wang, L., 2015. Integrated cortical structural marker for Alzheimer's disease. Neurobiol. Aging 36 (Suppl.1), S53–S59.
Montgomery, S.A., Asberg, M., 1979. A new depression scale designed to be sensitive to change. Br. J. Psychiatry 134, 382–389.
Perrot, M., Rivière, D., Mangin, J.-F., 2011. Cortical sulci recognition and spatial normalization. Med. Image Anal. 15, 529–550.
Plant, C., Teipel, S.J., Oswald, A., Böhm, C., Meindl, T., Mourao-Miranda, J., Bokde, A.W., Hampel, H., Ewers, M., 2010. Automated detection of brain atrophy patterns based on MRI for the prediction of Alzheimer's disease. Neuroimage 50, 162–174.
Reiner, P., Jouvent, E., Duchesnay, E., Cuingnet, R., Mangin, J.F., Chabriat, H., 2012. Alzheimer's Disease Neuroimaging Initiative. Sulcal span in Azheimer's disease, amnestic mild cognitive impairment, and healthy controls. J. Alzheimers Dis. 29, 605–613.
Reuter, M., Schmansky, N.J., Rosas, H.D., Fischl, B., 2012. Within-subject template estimation for unbiased longitudinal image analysis. Neuroimage 61, 1402–1418.
Sarazin, M., Berr, C., De Rotrou, J., Fabrigoule, C., Pasquier, F., Legrain, S., Michel, B., Puel, M., Volteau, M., Touchon, J., Verny, M., Dubois, B., 2007. Amnestic syndrome of the medial temporal type identifies prodromal AD: a longitudinal study. Neurology 69, 1859–1867.
Sarazin, M., Chauviré, V., Gerardin, E., Colliot, O., Kinkingnéhun, S., de Souza, L.C., Hugonot-Diener, L., Garnero, L., Lehéricy, S., Chupin, M., Dubois, B., 2010. The amnestic syndrome of hippocampal type in Alzheimer's disease: an MRI study. J. Alzheimers Dis. 22, 285–294.
Singh, V., Chertkow, H., Lerch, J.P., Evans, A.C., Dorr, A.E., Kabani, N.J., 2006. Spatial patterns of cortical thinning in mild cognitive impairment and Alzheimer's disease. Brain 129, 2885–2893.
Villemagne, V.L., Fodero-Tavoletti, M.T., Masters, C.L., Rowe, C.C., 2015. Tau imaging: early progress and future directions. Lancet Neurol. 14, 114–124.